ON THE PERFORMANCE ANALYSIS OF MOMENTUM METHOD: A FREQUENCY DOMAIN PERSPECTIVE

Anonymous authors
Paper under double-blind review

ABSTRACT

Momentum-based optimizers are widely adopted for training neural networks. However, the optimal selection of momentum coefficients remains elusive. This uncertainty impedes a clear understanding of the role of momentum in stochastic gradient methods. In this paper, we present a frequency domain analysis framework that interprets the momentum method as a time-variant filter for gradients, where adjustments to momentum coefficients modify the filter characteristics. Our experiments support this perspective and provide a deeper understanding of the mechanism involved. Moreover, our analysis reveals the following significant findings: high-frequency gradient components are undesired in the late stages of training; preserving the original gradient in the early stages, and gradually amplifying low-frequency gradient components during training both enhance generalization performance. Based on these insights, we propose Frequency Stochastic Gradient Descent with Momentum (FSGDM), a heuristic optimizer that dynamically adjusts the momentum filtering characteristic with an empirically effective dynamic magnitude response. Experimental results demonstrate the superiority of FSGDM over conventional momentum optimizers.

1 INTRODUCTION

Momentum has achieved great success in deep learning applications when combined with *Stochastic Gradient Descent* (SGD) (Robbins & Monro, 1951). Among various momentum methods (Polyak, 1964; Nesterov, 1983; Van Scoy et al., 2017; Ma & Yarats, 2018; Kidambi et al., 2018), one of the most prevalent variants is the momentum method utilized within *Stochastic Gradient Descent with Momentum* (SGDM) (Sutskever et al., 2013; Paszke et al., 2019), which can be expressed as:

$$\textbf{Standard-SGDM}\ \text{(decoupled)} : m_t = u_t m_{t-1} + v_t g_t, \quad x_t = x_{t-1} - \alpha_t m_t, \tag{1}$$

where g_t denotes the gradient at iteration t, m_t is the momentum buffer, and x_t represents the learnable parameters. The momentum coefficients u_t and v_t control the influence of the previous momentum and the current gradient, respectively, and α_t is the learning rate. For these time-variant momentum coefficients, a multistage setting has been commonly adopted in the machine learning community (Aybat et al., 2019; Kulunchakov & Mairal, 2019; Liu et al., 2020). Throughout this paper, we refer to this formulation, which decouples the two momentum coefficients, as Standard-SGDM. In contrast, another prevalent variant couples the two momentum coefficients using the *Exponential Moving Average* (EMA) method (Gardner Jr, 1985), leading to the formulation of EMA-SGDM:

$$\textbf{EMA-SGDM}\ \text{(coupled)} : m_t = u_t m_{t-1} + (1 - u_t) g_t, \quad x_t = x_{t-1} - \alpha_t m_t, \tag{2}$$

where $u_t \in [0, 1)$ is the momentum coefficient. Notably, this coupled momentum formulation is a special case of the decoupled one, i.e., Standard-SGDM with $v_t = 1 - u_t$. Our experiments show performance gaps between these two formulations. Moreover, how the momentum coefficients change over time can significantly affect the test accuracy (see Sec. 3). The existence of these two distinct momentum formulations and their differing performances raises two primary questions in modern deep learning:

1. **Decoupling vs. Coupling**: Should the coefficients u_t and v_t be decoupled or coupled?
2. **Temporal Variation**: How should the momentum coefficients evolve over time during training to achieve better model performance?

For Question 1, some literatures have investigated the convergence of the coupled method (Mai & Johansson, 2020; Li et al., 2022). Liu et al. (2020) argued that coupling the coefficients leads only to a constant scaling difference. Wang et al. (2024) further demonstrated that the mathematical equivalence between EMA-SGDM and Standard-SGDM can be achieved by adjusting the momentum coefficients and the learning rates in a coupled way. However, in practice, learning rate schedules are typically independent of momentum coefficient tuning during network training. On the other hand, popular frameworks like PyTorch (Paszke et al., 2019) adopt a decoupled momentum strategy by default. In our framework, we tackle the first question from the frequency domain perspective, revealing the relationship between the coupled and decoupled constructions.

Regarding Question 2, prior research offered diverse opinions on how the momentum coefficients should vary over time. Some studies preferred fixed decoupled momentum coefficients (Yan et al., 2018; Liu et al., 2018; Yu et al., 2019), commonly selecting u_t values as 0.9 and v_t value as 1. Liu et al. (2020) highlighted the benefits of stagewise learning rate schedules in EMA-SGDM, noting that u_t can either remain constant or increase along with the stagewise adjustments. Conversely, Smith (2018) demonstrated that decreasing the momentum coefficients while increasing the learning rate improves test performance. Moreover, Adaptive momentum methods (Kingma & Ba, 2014; Reddi et al., 2018; Luo et al., 2019; Chen et al., 2018) proved the convergence of decreasing coupled momentum coefficients in the context of online convex optimization. Nonetheless, a consensus regarding the optimal time-variant pattern of the momentum coefficients has yet to be reached.

To answer these questions, one has to understand how the momentum method affects the training process. Goh (2017) analyzed the momentum method from the aspect of convergence and dynamics. Several prior studies (Cutkosky & Orabona, 2019; Ma & Yarats, 2018) speculated that averaging past stochastic gradients through momentum might reduce the variance of the noise in the parameter update, thus making the loss decrease faster. Polyak (1964); Rumelhart et al. (1986) argued that the EMA momentum can cancel out oscillations along high-curvature directions and add up contributions along low-curvature directions. From the signal processing perspective, the EMA method acts as a discrete low-pass filter for smoothing out high-frequency fluctuations while retaining the low-frequency baseband pattern of the signal (Gardner Jr, 1985). These points of view bring us a new insight into connecting the momentum update processes with the specific filters. In this aspect, the momentum methods with different coefficient selections can be interpreted in a unified frequency domain analysis framework, whereby Questions 1 and 2 are resolved.

In this paper, we propose a novel frequency domain analysis framework to address the two questions and provide a deeper understanding of the role of momentum in stochastic optimization. To the best of our knowledge, this paper, for the first time, reveals the fundamental difference between Standard-SGDM and EMA-SGDM and uncovers the effects of the dynamic momentum coefficients clearly with the help of frequency domain analysis. Within our framework, high-frequency gradient components correspond to rapid fluctuations in gradient signals, while low-frequency gradient components represent smoother, gradual changes. Moreover, adjusting the momentum coefficients during training is equivalent to modifying the time-variant filtering characteristics of the momentum methods. This perspective not only explains the difference between various momentum methods but also provides practical guidelines for designing well-performed optimizers. Building upon these insights, we introduce the *Frequency Stochastic Gradient Descent with Momentum* (FSGDM) optimizer, which dynamically adjusts the momentum filter characteristics throughout training. Our experiments validate the effectiveness of FSGDM, showing that it outperforms conventional SGD-based momentum optimizers. The code will be released upon publication.

2 FREQUENCY DOMAIN ANALYSIS FRAMEWORK

This section introduces the background of Z-transform (Zadeh, 1950) in signal processing and then proposes a new frequency domain analysis framework for momentum methods.

2.1 Z-TRANSFORM AND QUASI-STATIONARY APPROXIMATION

Frequency analysis is a crucial technique for understanding how systems react to varying frequency components of input signals. Specifically, for discrete-time linear time-invariant systems, Z-transform is leveraged to examine how systems attenuate or amplify signals at specific frequencies, especially in the study of system stability, pole-zero behavior, etc. (Oppenheim et al., 1996).

Interestingly, in neural network training, the momentum update process at time t can be seen as a recursive filter where the gradient g_t and the momentum m_t act as input and output signals, respectively. The momentum coefficients affect the gradient adjustments across different frequency components. The high-frequency gradient components correspond to large and more abrupt changes in the gradient; while the low-frequency components indicate smooth and more gradual adjustments.

However, one key issue is that our momentum method can be inherently time-variant, as its coefficients may change stagewise throughout the training process. This variability makes it difficult to apply traditional Z-transform analysis. To overcome this, inspired by the Zadeh (1961); Jury (1964), we approximate the system as time-invariant in each discrete interval stage. By holding the momentum coefficients constant over every interval, we construct a time-invariant quasi-stationary system (Hubner & Tran-Gia, 1991), enabling us to apply the Z-transform validly.

In our following analysis framework and our later optimizer design, we follow this multistage strategy for changing momentum coefficients. Particularly, for a predefined stage whose length is denoted by δ, the momentum coefficients are redefined using the floor function to ensure they remain constant over the whole stage:

$$u_t = u(\lfloor t/\delta \rfloor \times \delta) \quad \text{and} \quad v_t = v(\lfloor t/\delta \rfloor \times \delta), \tag{3}$$

where $u(t), v(t)$ are the continuous dynamic sequence functions with respect to t. While there are multiple sequences with different designs, in this paper, we use the following increasing and decreasing sequences:

$$\text{Increasing} : u(t) \text{ or } v(t) = \frac{t}{t+\mu}, \quad \text{Decreasing} : u(t) \text{ or } v(t) = 1 - \frac{t+1}{t+\nu}, \tag{4}$$

where μ and ν are the increasing and decreasing factors [1]. In App. B.1, we also examined the test set performance using other kinds of dynamic sequences. Under the above settings, for a given stage k $(k = 1, \cdots, N)$, with $t \in [(k-1)\delta, k\delta - 1]$, the *momentum system* [2] becomes:

$$m_t = u_k m_{t-1} + v_k g_t \tag{5}$$

where $u_k = u((k-1)\delta)$ and $v_k = v((k-1)\delta)$ are constants for the duration of the k-th stage. Additionally, we set the total number of stages, denoted by N, to a constant value of 300 for all the experiments in this paper.

2.2 FREQUENCY DOMAIN ANALYSIS OF THE MOMENTUM METHOD

In this subsection, we introduce our frequency domain analysis framework and analyze the impacts of the momentum method on neural network training. We first apply Z-transform, denoted by $\mathcal{Z}$, to Eqn. 5:

$$M(z) = u_k z^{-1} M(z) + v_k G(z), \tag{6}$$

where $G(z) = \mathcal{Z}\{g_t\}$, $M(z) = \mathcal{Z}\{m_t\}$, and $z^{-1}M(z) = \mathcal{Z}\{m_{t-1}\}$. To obtain the frequency response of the momentum system during stage k, we evaluate the transfer function $H_k(z)$ on the unit circle (Oppenheim et al., 1996):

$$H_k(z) = \frac{M(z)}{G(z)} = \frac{v_k}{1 - u_k z^{-1}} \quad \xRightarrow{z=e^{j\omega}} \quad H_k(\omega) = \frac{v_k}{1 - u_k e^{-j\omega}}, \tag{7}$$

where $\omega \in [0, \pi]$ is the normalized angular frequency of the real-value signal. The frequency response of the momentum system describes how the input gradient signal $G(z)$ is altered to the output momentum signal $M(\omega)$ when it passes through the system. Note that this transfer function is valid for the entire duration of the k-th quasi-stationary stage.

Magnitude Response. The magnitude response of the momentum system in the k-th stage can be calculated by taking the magnitude of $H_k(\omega)$:

$$|H_k(\omega)| = \frac{|v_k|}{\sqrt{1 - 2u_k \cos\omega + u_k^2}}. \tag{8}$$

---

[1] Note that different from the increasing sequence, the numerator of the decreasing sequence is $t+1$. This design avoids the zero gradients at the first training stage.

[2] In this paper, momentum system refers to the momentum update process.

The magnitude response describes the amplitude scaling effect of the system at different frequencies. It indicates how the momentum system amplifies or attenuates different frequency components during each stage. This characteristic of the momentum system plays a key role in affecting the optimization process. Notably, when $|H_k(\omega)| < 1$, the momentum system attenuates the signals with frequency ω; when $|H_k(\omega)| > 1$, the momentum system amplifies the signals with ω. Consequently, we divide the momentum systems into two categories: *Orthodox Momentum Systems* and *Unorthodox Momentum Systems*.

Orthodox Momentum Systems are the ones whose amplitude of the magnitude response will not surpass 1, like the EMA-SGDM (2). This kind of momentum system only shows attenuating characteristics. Specifically, the momentum system behaves as a **low-pass** filter when $u_k > 0$ and a **high-pass** filter when $u_k < 0$. Additionally, when u_k gets close to 1, the momentum system will prefer to attenuate the gradient components with high frequencies. The visualization of the (dynamic) magnitude responses of orthodox momentum systems is in Sec. 3.1 and App. B.2.

For *Unorthodox Momentum Systems* where the amplitude of magnitude response will surpass 1, such as selecting $u_t = 0.9$ and $v_t = 1$ in Standard-SGDM (1), the momentum system possesses both amplifying and attenuating characteristics. In this paper, we refer to these kinds of unorthodox filters as **low/high-pass gain** filters. Specifically, the momentum system behaves as a low-pass gain filter when $u_k > 0, v_k = 1$ and a high-pass gain filter when $u_k < 0, v_k = 1$. Additionally, if u_k is close to 1, the momentum system attenuates high-frequency gradient components while strongly amplifying low-frequency components; if u_k is close to -1, the momentum system attenuates low-frequency gradient components while strongly amplifying high-frequency components. The visualization of the (dynamic) magnitude responses of unorthodox momentum systems is in Sec. 3.2 and App. B.2.

To demonstrate the momentum effects from the frequency perspective, in Fig. 1, we compare an original sinusoidal signal, a noisy version injected with Gaussian noise, and the signal after applying the momentum method (which is called momentum signal for short) in the time domain. The red curve represents the noisy signal, the black dashed curve corresponds to the original noise-free true signal, and the cyan curve shows the momentum signal. We can see that different selections of u_k and v_k significantly affect the amplifying or attenuating effects of the momentum system.

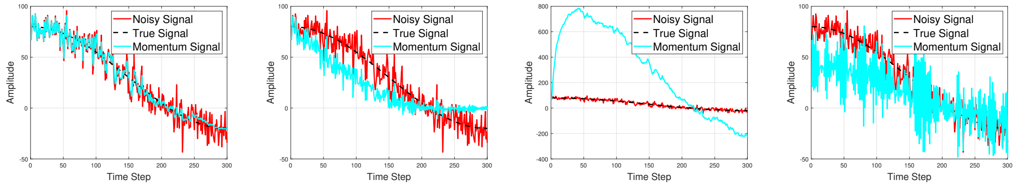

(a) Dynamic Low-pass Filter (b) Dynamic High-pass Filter (c) Low-pass Gain Filter (d) High-pass gain Filter

Figure 1: Visualization of different filters towards the noisy sinusoidal signal. (a) $u_k = 0 \to 1, v_k = 1 - u_k$, with the system gradually shifting from an all-pass filter to a narrow low-pass filter; (b) $u_k = 0 \to -1, v_k = 1 + u_k$, with the system gradually shifting from an all-pass filter to a narrow high-pass filter; (c) $u_k = 0.9, v_k = 1$, which indicates the momentum behaves like a low-pass gain filter with amplification on low-frequency gradient components; (d) $u_k = -0.9, v_k = 1$, which indicates the momentum behaves like a high-pass gain filter with amplification on high-frequency components. The amplifying and attenuating effects of different momentum systems are verified.

Phase Response. We also have the phase response of the momentum system in the k-th stage,

$$\arg(H_k(\omega)) = \arg(v_k) - \tan^{-1}\left(\frac{u_k \sin\omega}{1 - u_k \cos\omega}\right), \tag{9}$$

where $\arg(\cdot)$ is the argument operator. For any real value v_k, $\arg(v_k) = 0$ if $v_k > 0$ and $\arg(v_k) = \pi$ if $v_k < 0$; for any $\omega \in [0, \pi]$ and $u_k \in (-1, 1)$, $\tan^{-1}(u_k \sin\omega/(1 - u_k \cos\omega)) \in (-\frac{\pi}{2}, \frac{\pi}{2})$. The phase response describes the phase-shifting effect of the momentum system at different frequencies. In the context of gradient-based optimization, the phase shift indicates a change in the optimization direction. Therefore, when $v_k < 0$, the phase shift of the momentum adds up an extra π rad on the shifted direction, indicating that the direction of the update is greatly reversed, which can lead to oscillations, instability, or divergence in the optimization process. Thus, it is necessary to select a positive v_k when applying momentum methods.

While the phase response of the momentum only provides limited insights, understanding the behavior of the magnitude response across stages is essential for analyzing the time-variant characteristics of the momentum system. By plotting the dynamic magnitude response value $|H_k(\omega)|$ on the normalized angular frequency axis for each stage k, we can track how the frequency-dependent behavior of the multistage momentum system evolves over time. This provides valuable insights into the amplifying or attenuating characteristics of the momentum system. Further results on the comparisons of momentum systems with different dynamic magnitude responses are presented in the next section.

3 DYNAMIC MAGNITUDE RESPONSE OF THE MOMENTUM SYSTEMS

In this section, we present an empirical study to discover the influence of the momentum coefficients by comparing the test performance on momentum systems with different dynamic magnitude responses. We train VGG (Simonyan & Zisserman, 2014) on the CIFAR-10 (Krizhevsky et al., 2009) dataset and ResNet50 (He et al., 2016) on the CIFAR-100 dataset using different momentum coefficients, while keeping all other hyperparameters unchanged. For each experiment, we report the mean and standard error (as subscripts) of test accuracy for 3 runs with random seeds from 0-2. The detailed experimental settings can be found in App. C. The experimental results in CIFAR-10 show high similarity to those in CIFAR-100. Thus, here, we mainly focus on the analysis based on CIFAR-100 and defer the experimental results of VGG16 on CIFAR-10 in App. B.3.

3.1 ORTHODOX MOMENTUM SYSTEMS

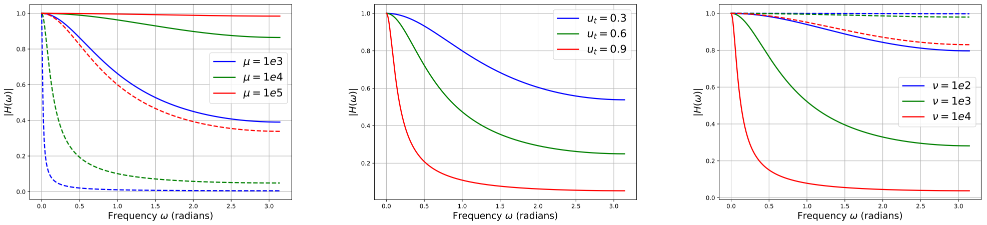

(a) Dynamic Magnitude Response (b) Magnitude Response (c) Dynamic Magnitude Response

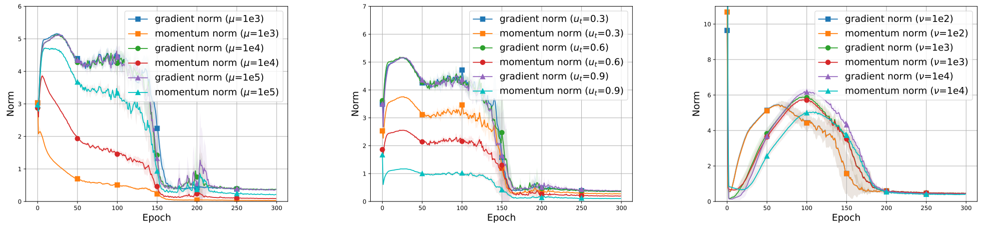

(d) Norm Comparisons (e) Norm Comparisons (f) Norm Comparisons

Figure 2: (**Up**) Analysis of the (dynamic) magnitude responses in the early and late training stages for EMA-SGDM with low-pass momentum defined in Eqn. 10. The *solid lines* denote the magnitude responses in the *early stages*, and the *dashed lines* denote the magnitude responses in the *late stages*. (**Down**) The comparison between the gradient norms and momentum norms for EMA-SGDM with low-pass momentum. Left Column: increasing sequence. Middle Column: fixed sequence. Right Column: decreasing sequence.

We first focus on the orthodox momentum systems with the following two main types: low-pass and high-pass momentum, defined as:

$$\textbf{Low-pass}: m_t = u_t m_{t-1} + (1-u_t)g_t, \quad \textbf{High-pass}: m_t = -u_t m_{t-1} + (1-u_t)g_t, \tag{10}$$

where $u_t \in [0, 1)$ can be set as increasing, decreasing sequences, or fixed value. For time-variant momentum systems, different strategies of u_t result in different time-variant filtering characteristics during training. According to Sec. 2.1, scaling the increasing and decreasing factors affects the changing rates of u_t. In the following, we demonstrate the dynamic magnitude responses, comparisons between gradient norms and momentum norms, and test accuracy results of orthodox momentum systems under different u_t sequences [3].

Example 1: Low-Pass Momentum. We first explore the effect of increasing, fixed, and decreasing u_t sequences in low-pass momentum. Fig. 2(a) - 2(c) show the corresponding dynamic magnitude responses over time. With increasing u_t, the system transits from an all-pass to a progressively narrower low-pass filter, gradually attenuating high-frequency components. Larger μ results in slower transitions. Decreasing u_t shows a reverse behavior, with larger ν resulting in slower transitions. u_t with a fixed value maintains a constant filter, with larger u_t leading to more aggressive smoothing and noise reduction characteristics. The norm comparisons in Fig. 2(d) - 2(f) show that the momentum norms in low-pass momentum systems are always less than the corresponding gradient norms. Larger u_t, ν and smaller μ lead to more reduced momentum norms, which validates the time-variant filtering characteristics of orthodox momentum systems.

Test accuracy results in Table 1 reveal that increasing or fixing u_t can achieve higher accuracy compared to applying decreasing sequences of u_t. In particular, momentum systems with proper increasing sequences of u_t can outperform those with fixed u_t. We also find that larger ν results in poorer model performance. These phenomena indicate that gradually attenuating high-frequency components during training improves test set performance, while excessive suppression of low-frequency gradient components in early stages and retention of high-frequency components in late stages degrade model performance.

Example 2: High-Pass Momentum. High-pass momentum systems exhibit symmetric dynamic magnitude responses and similar norm comparisons, compared to their low-pass counterparts (see Fig. 6 in App. B.2). With increasing u_t, the system shifts from an all-pass to a narrow high-pass filter, progressively attenuating low-frequency components. Decreasing sequences act in reverse. Fixed sequences with larger u_t lead to more aggressive attenuation of low-frequency components. The comparison of gradient norms and momentum norms can be found in App. B.2.

Test accuracy in Table 1 shows that dynamic high-pass systems with larger μ and smaller ν yield better top-1 accuracy performance. When selecting fixed values, momentum systems with larger u_t perform more poorly. These results confirm that suppressing low-frequency gradient components is harmful. Moreover, high-pass systems generally outperform low-pass systems when applying decreasing strategies with the same ν, suggesting that high-frequency components play a crucial role in the early training stages, which is also supported by the studies in App. B.4.

From Examples 1 and 2, we empirically verify that high-frequency gradient components are detrimental in late training stages, while their preservation in early stages leads to higher test accuracy, which matches the viewpoint that gradient noise has a generalization benefit early in training (Smith et al., 2020).

Table 1: Top-1 ACC. (%) comparisons of different momentum coefficient strategies of orthodox momentum systems of ResNet50 on CIFAR-100.

	Increasing Factor (μ)			Fixed Value (u_t)			Decreasing Factor (ν)		
Parameters	1k	10k	100k	0.3	0.6	0.9	100	1k	10k
Low-pass	$77.12_{0.07}$	$77.06_{0.14}$	$76.86_{0.12}$	$76.98_{0.09}$	$76.82_{0.18}$	$76.84_{0.06}$	$72.58_{0.44}$	$70.53_{0.31}$	$69.69_{0.75}$
High-pass	$51.59_{0.78}$	$67.55_{0.22}$	$74.72_{0.06}$	$72.46_{0.13}$	$65.14_{0.17}$	$53.43_{0.26}$	$76.82_{0.25}$	$75.92_{0.12}$	$70.99_{0.18}$

3.2 UNORTHODOX MOMENTUM SYSTEMS

Unorthodox momentum systems allow magnitude responses larger than 1, meaning they can both attenuate and amplify gradients in different frequency bands. We focus on two main types: low-pass gain and high-pass gain momentum, defined as:

$$\textbf{Low-pass gain}: m_t = u_t m_{t-1} + g_t, \quad \textbf{High-pass gain}: m_t = -u_t m_{t-1} + g_t, \tag{11}$$

where $u_t \in [0, 1)$ can follow increasing, fixed, or decreasing sequences. For simplification reasons, we use the PyTorch setting with $v_t = 1$. We show the dynamic magnitude responses, comparisons between gradient norms and momentum norms, and test accuracy results of unorthodox momentum systems under different u_t sequences as follows.

---

[3] Note that selecting $\mu = 100$ and $\nu = 10^4$ lead to a long stage of super narrow-band filter. To avoid this problem, we select $\mu = 10^3, 10^4, 10^5$ and $\nu = 10^2, 10^3, 10^4$ in this paper.

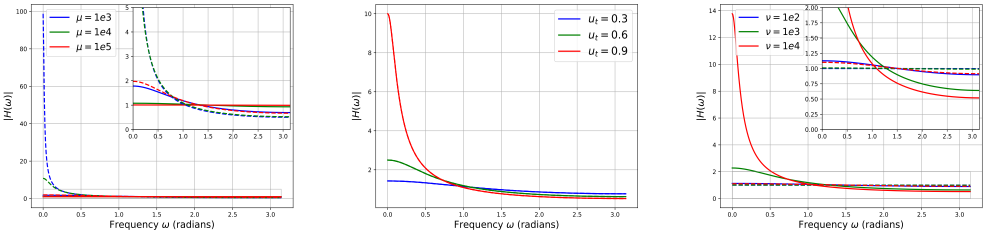

(a) Dynamic Magnitude Response (b) Magnitude Response (c) Dynamic Magnitude Response

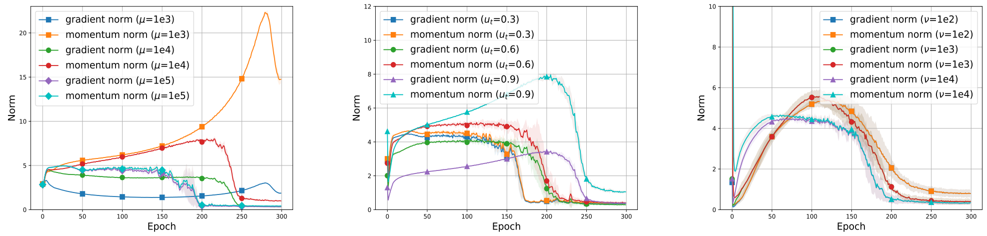

(d) Norm Comparisons (e) Norm Comparisons (f) Norm Comparisons

Figure 3: (**Up**) Analysis of the (dynamic) magnitude responses in the early and late training stages for Standard-SGDM with low-pass gain momentum defined in Eqn. 11. The *solid lines* denote the magnitude responses in the *early stages*, and the *dashed lines* denote the magnitude responses in the *late stages*. (**Down**) The comparison between the gradient norms and momentum norms for Standard-SGDM with low-pass gain momentum. Left Column: increasing sequence. Middle Column: fixed sequence. Right Column: decreasing sequence.

Example 3: Low-Pass Gain Momentum. In low-pass gain momentum, the system transits from an all-pass to a narrower low-pass gain filter as u_t increases, amplifying low-frequency components while attenuating high-frequency components. Fig. 3(a) - 3(c) show the corresponding dynamic magnitude responses over time. A large μ corresponds to the slow shifts. Decreasing u_t reverses the trend, heavily amplifying low-frequency components early and relaxing this effect over time. Fixed u_t maintains constant filters, in which larger u_t amplifies low-frequency components more aggressively. Fig. 3(d) - 3(f) demonstrate larger momentum norms compared to gradient norms, indicating the amplification effects in gain filters. Larger u_t, ν and smaller μ lead to more reduced momentum norms, which validates the time-variant filtering characteristics of orthodox momentum systems. Test results in Table 2 indicate that increasing u_t with appropriate μ outperforms the scenarios using fixed and decreasing sequences of u_t. We also find that smaller ν yields worse accuracy in test sets. From these results, we conclude that amplifying low-frequency gradient components and attenuating high-frequency ones in a proper way, improves test set performance.

Example 4: High-Pass Gain Momentum. High-pass gain momentum mirrors the dynamic magnitude response behavior of low-pass gain systems (see Fig. 7 in App B.2). Increasing u_t gradually amplifies high-frequency gradient components and attenuates low-frequency ones. Decreasing u_t reverses this pattern, heavily amplifying high-frequency components early on. Fixed constructions more aggressively amplify high-frequency components for larger u_t. The comparison of gradient norms and momentum norms can be found in App. B.2. Test accuracy in Table 2 shows that fixed constructions with larger u_t and decreasing u_t with larger ν perform worse. These findings confirm that amplifying high-frequency gradients in training might be undesirable.

From Examples 3 and 4, we empirically verify that proper amplification in unorthodox momentum systems can improve model performance, particularly when amplifying low-frequency gradient components.

Table 2: Top-1 ACC. (%) comparisons of different momentum coefficient strategies of unorthodox momentum systems of ResNet50 on CIFAR-100.

	Increasing Factor (μ)			Fixed Value (u_t)			Decreasing Factor (ν)		
Parameters	1k	10k	100k	0.3	0.6	0.9	100	1k	10k
Low-Pass Gain	$76.10_{0.14}$	$80.48_{0.03}$	$78.02_{0.03}$	$78.01_{0.04}$	$79.51_{0.15}$	$79.71_{0.25}$	$70.37_{0.67}$	$71.53_{0.62}$	$76.18_{0.38}$
High-Pass Gain	$75.47_{0.21}$	$74.54_{0.16}$	$75.97_{0.27}$	$75.68_{0.18}$	$74.56_{0.09}$	$73.77_{0.18}$	$76.41_{0.41}$	$74.00_{0.26}$	$68.90_{0.82}$

3.3 DISCUSSION

The differences in norm comparison and test accuracy between orthodox and unorthodox momentum systems validate the distinction between EMA-SGDM and Standard-SGDM from the signal processing perspective. EMA-SGDM only possesses attenuating filter effects, while Standard-SGDM can, at the same time, amplify and attenuate different frequency gradient components. Moreover, we show that Standard-SGDM with proper momentum coefficients can consistently outperform EMA-SGDM. These results clarify the difference between coupled and decoupled momentum coefficients and indicate that decoupling the momentum coefficients is usually beneficial, which answers Question 1.

Regarding Question 2, the test results show that decoupled momentum coefficients with a properly increasing u_t and fixed v_t can achieve better performance. In particular, our empirical findings reveal the following insights in training *Convolutional Neural Networks* (CNNs): 1) high-frequency gradient components are undesired in the late stages of training; 2) preserving the original gradient in the early stages leads to improved test set accuracy; 3) gradually amplifying low-frequency gradient components enhance the generalization performance. Furthermore, we find that these insights are also adaptable in various learning areas (see Sec. 5). Based on these insights, it may be possible to design a more effective optimizer by appropriately adjusting the momentum coefficients.

4 FREQUENCY-BASED OPTIMIZER

As suggested by our frequency domain analysis framework, achieving better test performance is equivalent to finding an appropriate dynamic filter-changing pattern for momentum systems. Based on this idea, we propose FSGDM, a heuristic optimizer that dynamically adjusts momentum filtering characteristics. Furthermore, in order to explore the potential optimal strategies of our proposed FSGDM based on the findings in Sec. 3.3, several sets of experiments in various deep-learning tasks are conducted.

4.1 FREQUENCY STOCHASTIC GRADIENT DESCENT WITH MOMENTUM

```
Algorithm 1: FSGDM
Input: $\Sigma$, $c$, $v$, $N$;
Initialization: $m_0$, $\mu = c\Sigma$,
  $\delta = \Sigma/N$;
for each $t = 1, 2, \ldots$ do
    $g_t = \nabla\mathcal{L}_t(x_{t-1}, \zeta_{t-1})$;
    $u(t) = \frac{t}{t+\mu}$,    $u_t = u(\lfloor t/\delta \rfloor \times \delta)$;
    $m_t = u_t m_{t-1} + v g_t$;
    $x_t = x_{t-1} - \alpha_t m_t$;
end
```

Generally, determining the *best* optimization strategy by tuning u_t and v_t according to our frequency domain analysis is challenging. In the field of signal processing, how to select the best filters for different problems is still an open problem. However, we can design a *better* optimizer based on the findings in Sec. 3.3. Still, there are infinite dynamic magnitude responses that can meet the requirements of the aforementioned findings. Based on Occam's Razor principle, we provide a minimalist form of our proposed optimizer in Algorithm 1, where Σ is the total gradient update steps in the whole training process determined by the epoch number and the size of the dataset, c is a scaling factor, $\mathcal{L}_t : \mathbb{R}^d \to \mathbb{R}$ is the loss for the t-th step, ζ_{t-1} denotes a minibatch drawn from the training data, and N is the number of stages. μ and v are adjustable parameters that dominate the filtering characteristic of FSGDM. Moreover, since μ is a function of Σ, the dynamic magnitude response can be inherited when Σ varies. In particular, we have the following proposition.

Proposition 1. *By fixing the number of stages N and the scaling factor c, the dynamic magnitude response of Algorithm 1 keeps invariant with respect to changes in the total number of training steps.*

The proof of Proposition 1 is deferred in App. A.3. By this, we show that the dynamic magnitude response of a well-performed FSGDM can be adaptable to various tasks. In the following subsection, we explore the optimal scaling factor c and momentum coefficient v for FSGDM.

4.2 EMPIRICAL EXPLORATION OF OPTIMAL SETTINGS FOR FSGDM

As discussed in Sec. 3, different choices of c and v can significantly affect the filtering characteristics of FSGDM. To understand their impact on optimization performance and to identify optimal parameter settings, we conduct a comprehensive empirical study.

Specifically, we empirically explore the optimal parameter selection of FSGDM across three different image classification tasks by first sweeping c and v within the ranges of $(0, 1)$ and $[0.5, 3]$, respectively. Specifically, we conduct three sets of experiments using the same codebase (See App. C for more training details): (1) training ResNet18 for 100 epochs on CIFAR-10, (2) training ResNet34 for 100 epochs on Tiny-ImageNet (Le & Yang, 2015), and (3) training ResNet50 for 300 epochs on CIFAR-100. We also explore the optimal parameter selection on one natural language processing task in App. B.7. By finding the parameter selections with better test performance in different tasks, we try to empirically summarize the law of optimal parameter selection.

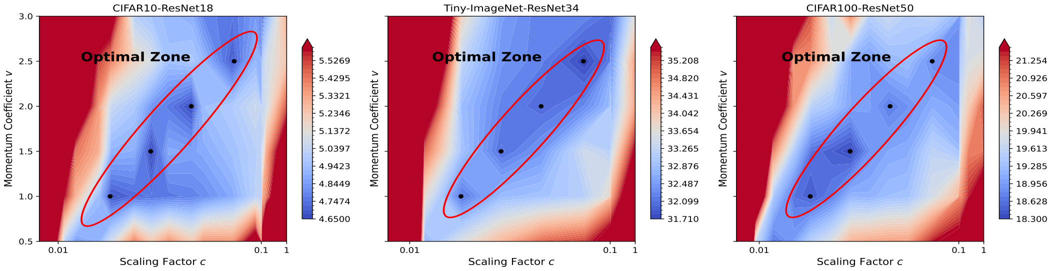

Figure 4: The Top-1 test errors of training ResNet18 on CIFAR-10, ResNet34 on Tiny-ImageNet and ResNet50 on CIFAR-100. The results show that the optimal parameter selections across these three training settings exhibit a high similarity. The black points denote the parameter selections with better test performance. The optimal zone of the parameter selection is circled in red.

The results in Fig. 4 show that there exists an optimal zone where relatively better test accuracy results can be achieved. When the momentum coefficient v is fixed, the test accuracy shows an initial increase followed by a decline as the scaling factor c increases. In App. B.8, we plot the magnitude responses and the test accuracy results of the black points in Fig. 4 and find that these parameter selections have similar dynamic magnitude responses and test accuracy curves. Thus, we assume the parameter selections with similar dynamic magnitude responses will lead to close performance. More discussions are in App. B.8.

5 EXPERIMENTS

To verify the generalization of the proposed FSGDM, we perform a large-scale comparison across vision classification tasks, natural language processing (NLP) tasks and reinforcement learning (RL) tasks. We compare the test performance of FSGDM and conventional SGD-based momentum optimizers, including Standard-SGDM and EMA-SGDM. We set $u_t = 0.9, v_t = 1$ for Standard-SGDM, and $u_t = 0.9$ for EMA-SGDM, which are the common momentum coefficient selections in training neural networks. For a fair comparison and convenience, we set $c = 0.033, v = 1$, which is one of the black points in the optimal zone in Fig. 4, for FSGDM. Note that other combinations of c and v in the optimal zone can also be selected. For the other adjustable parameters in Algorithm 1, we set N to 300 as mentioned at the end of Sec. 2.1, and set Σ as the number of total training steps. Notably, since our focus is on comparing the performance of different optimizers, we do not fine-tune every parameter for each individual model but use the same hyperparameters across all models for convenience. See App. C for more experimental details.

Table 3: Performance on Image Classification Experiments

Dataset	CIFAR-10		CIFAR-100		Tiny-ImageNet		ImageNet
Model	VGG16	ResNet18	ResNet50	DenseNet121	ResNet34	MobileNet	ResNet50
EMA-SGDM	$93.71_{0.07}$	$94.19_{0.07}$	$76.84_{0.06}$	$76.18_{0.23}$	$62.28_{0.17}$	$55.00_{0.10}$	$74.24_{0.04}$
Standard-SGDM	$94.08_{0.07}$	$95.57_{0.06}$	$79.71_{0.25}$	$80.49_{0.09}$	$67.51_{0.08}$	$58.31_{0.20}$	$76.66_{0.09}$
FSGDM	$\mathbf{94.19}_{0.07}$	$\mathbf{95.66}_{0.07}$	$\mathbf{81.44}_{0.06}$	$\mathbf{81.14}_{0.05}$	$\mathbf{67.74}_{0.06}$	$\mathbf{59.61}_{0.11}$	$\mathbf{76.91}_{0.05}$

CNNs on Image Classification. We perform four sets of experiments with different datasets in computer vision tasks and use various CNN architectures for training them. Specifically, we select: (a) VGG16 and ResNet18 for CIFAR-10; (b) ResNet50 and DenseNet121 (Huang et al., 2017) for CIFAR-100; (c) ResNet34 and MobileNet (Howard, 2017) for Tiny-ImageNet; (d) ResNet50 for ILSVRC 2012 ImageNet Russakovsky et al. (2015). For each task, we report the mean and standard error (as subscripts) of test accuracy for 3 runs with random seeds from 0-2. The results in Table 3 show that our FSGDM consistently achieves better test set performance. Additionally, we can observe that Standard-SGDM steadily outperforms EMA-SGDM, which aligns with our discoveries in Sec. 3.3.

Natural Language Processing (NLP). We conducte experiments on the IWSLT14 German-English translation task (Cettolo et al., 2014) to represent NLP tasks, a widely used benchmark in the community. Specifically, we train six different models encompassing a variety of architectures: two convolution-based models, FConv (Gehring et al., 2017) and LightConv (Wu et al., 2019); two LSTM-based models, vanilla LSTM (Hochreiter et al., 1997) and an LSTM variant, LSTM-W (Wiseman & Rush, 2016); and two Transformer-based models (Vaswani et al., 2017) with different sizes, Transformer-tiny and Transformer. Model performance is reported using BLEU scores, where higher scores indicate better performance, and we summarize all results in Table 4. Compared with the baseline optimizers, the proposed FSGDM outperforms all others in this task across six different models. This shows the effectiveness of our optimizer in improving translation quality. Moreover, the consistent improvement highlights the robustness of FSGDM and its ability to generalize across different neural network structures in natural language processing tasks.

Table 4: Performance on IWSLT14 Dataset

Model	FConv	LightConv	LSTM	LSTM-W	Transformer-tiny	Transformer
EMA-SGDM	13.97$_{0.01}$	10.56$_{0.01}$	4.99$_{0.01}$	1.20$_{0.07}$	5.17$_{0.01}$	6.27$_{0.01}$
Standard-SGDM	27.41$_{0.02}$	33.05$_{0.04}$	28.12$_{0.06}$	24.66$_{0.06}$	18.16$_{0.03}$	31.50$_{0.05}$
FSGDM	**28.30$_{0.01}$**	**33.44$_{0.02}$**	**29.27$_{0.02}$**	**27.41$_{0.03}$**	**19.94$_{0.07}$**	**32.40$_{0.05}$**

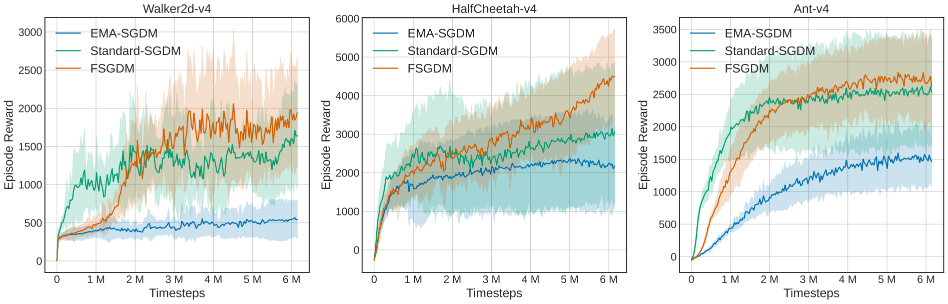

Figure 5: The reward curves of EMA-SGD, Standard-SGD and FSGDM on three MuJoCo tasks.

Reinforcement Learning (RL). We evaluate FSGDM on PPO (Schulman et al., 2017), one of the most popular policy gradient methods in reinforcement learning. We replace the default Adam optimizer (Kingma & Ba, 2014) in PPO with FSGDM, Standard-SGDM and EMA-SGDM. We test the three optimizers on Walked2d-v4, HalfCheetah-v4 and Ant-V4, which are actually continuous control environments simulated by the standard and widely-used engine, MuJoCo (Todorov et al., 2012). Following standard evaluation, we run each game under 10 random seeds (range from 0-9), and test the performance for 10 episodes every 30,000 steps. All experiments are conducted using the Tianshou codebase (Weng et al., 2022), a widely known RL framework. Fig. 5 presents the results on three tasks, where the solid line represents the average episode rewards during evaluation, and the shaded region indicates the 75% confidence interval. It can be easily observed that on three test games, our FSGDM achieves the highest rewards than Standard-SGDM and EMA-SGDM.

6 CONCLUSIONS

This paper proposes a frequency domain analysis framework for the momentum method. Based on the proposed framework, we find that different selections of momentum coefficients correspond to different filter characteristics of the momentum methods. The generalization performance will be significantly distinct under different time-variant momentum coefficients. Furthermore, we develop a heuristic optimizer named FSGDM which outperforms the conventional SGD-based momentum optimizers in various learning tasks. Future work may investigate how we can achieve the *best* filtering strategy for all the general scenarios in a more theoretical way. Moreover, extending the frequency domain analysis framework to other second-moment optimizers like RMSprop (Tieleman & Hinton, 2012) and Adam is also an interesting topic.

REFERENCES

Necdet Serhat Aybat, Alireza Fallah, Mert Gurbuzbalaban, and Asuman Ozdaglar. A universally optimal multistage accelerated stochastic gradient method. *Advances in Neural Information Processing Systems*, 32, 2019.

Mauro Cettolo, Jan Niehues, Sebastian Stüker, Luisa Bentivogli, and Marcello Federico. Report on the 11th iwslt evaluation campaign. In *Proceedings of the 11th International Workshop on Spoken Language Translation: Evaluation Campaign*, pp. 2–17, 2014.

Xiangyi Chen, Sijia Liu, Ruoyu Sun, and Mingyi Hong. On the convergence of a class of adam-type algorithms for non-convex optimization. *International Conference on Learning Representations*, 2018.

Ashok Cutkosky and Francesco Orabona. Momentum-based variance reduction in non-convex sgd. *Advances in Neural Information Processing Systems*, 32, 2019.

Everette S. Gardner Jr. Exponential smoothing: The state of the art. *Journal of forecasting*, 4(1): 1–28, 1985.

Jonas Gehring, Michael Auli, David Grangier, Denis Yarats, and Yann N Dauphin. Convolutional sequence to sequence learning. In *International Conference on Machine Learning*, pp. 1243–1252. PMLR, 2017.

Gabriel Goh. Why momentum really works. *Distill*, 2017. doi: 10.23915/distill.00006.

Kaiming He, Xiangyu Zhang, Shaoqing Ren, and Jian Sun. Delving deep into rectifiers: Surpassing human-level performance on imagenet classification. In *Proceedings of the IEEE international conference on computer vision*, pp. 1026–1034, 2015.

Kaiming He, Xiangyu Zhang, Shaoqing Ren, and Jian Sun. Deep residual learning for image recognition. In *Proceedings of the IEEE conference on computer vision and pattern recognition*, pp. 770–778, 2016.

Sepp Hochreiter, , and Juergen Schmidhuber. Long short-term memory. *Neural Computation*, 1997.

Andrew G. Howard. Mobilenets: Efficient convolutional neural networks for mobile vision applications. *arXiv preprint arXiv:1704.04861*, 2017.

Gao Huang, Zhuang Liu, Laurens Van Der Maaten, and Kilian Q. Weinberger. Densely connected convolutional networks. In *Proceedings of the IEEE conference on computer vision and pattern recognition*, pp. 4700–4708, 2017.

F Hubner and Phuoc Tran-Gia. Quasi-stationary analysis of a finite capacity asynchronous multiplexer with modulated deterministic input. *ITC-13, Copenhagen*, 1991.

Eliahu Ibrahim Jury. Theory and application of the z-transform method. *Electronics and Power*, 11 (3):291–299, 1964.

Rahul Kidambi, Praneeth Netrapalli, Prateek Jain, and Sham Kakade. On the insufficiency of existing momentum schemes for stochastic optimization. In *2018 Information Theory and Applications Workshop (ITA)*, pp. 1–9. IEEE, 2018.

Diederik P. Kingma and Jimmy Lei Ba. Adam: A method for stochastic optimization. *International Conference on Learning Representations*, 2014.

Alex Krizhevsky, Geoffrey Hinton, et al. Learning multiple layers of features from tiny images. *Master's thesis, Department of Computer Science, University of Toronto*, 2009.

Andrei Kulunchakov and Julien Mairal. A generic acceleration framework for stochastic composite optimization. *Advances in Neural Information Processing Systems*, 32, 2019.

Ya Le and Xuan Yang. Tiny imagenet visual recognition challenge. *CS 231N*, 7(7):3, 2015.

Xiaoyu Li, Mingrui Liu, and Francesco Orabona. On the last iterate convergence of momentum methods. In *International Conference on Algorithmic Learning Theory*, pp. 699–717. PMLR, 2022.

Tianyi Liu, Zhehui Chen, Enlu Zhou, and Tuo Zhao. A diffusion approximation theory of momentum SGD in nonconvex optimization. *arXiv preprint arXiv:1802.05155*, 2018.

Yanli Liu, Yuan Gao, and Wotao Yin. An improved analysis of stochastic gradient descent with momentum. In H. Larochelle, M. Ranzato, R. Hadsell, M.F. Balcan, and H. Lin (eds.), *Advances in Neural Information Processing Systems*, volume 33, pp. 18261–18271. Curran Associates, Inc., 2020.

Ilya Loshchilov and Frank Hutter. SGDR: Stochastic gradient descent with warm restarts. *International Conference on Learning Representations*, 2016.

Liangchen Luo, Yuanhao Xiong, Yan Liu, and Xu Sun. Adaptive gradient methods with dynamic bound of learning rate. *International Conference on Learning Representations*, 2019.

Jerry Ma and Denis Yarats. Quasi-hyperbolic momentum and adam for deep learning. In *International Conference on Learning Representations*, 2018.

Vien Mai and Mikael Johansson. Convergence of a stochastic gradient method with momentum for non-smooth non-convex optimization. In *International Conference on Machine Learning*, pp. 6630–6639. PMLR, 2020.

Yurii Nesterov. A method for solving the convex programming problem with convergence rate o (1/k2). In *Dokl akad nauk Sssr*, volume 269, pp. 543, 1983.

Alan V. Oppenheim, Alan S. Willsky, and S. Hamid Nawab. *Signals & systems (2nd ed.)*. Prentice-Hall, Inc., USA, 1996. ISBN 0138147574.

Adam Paszke, Sam Gross, Francisco Massa, Adam Lerer, James Bradbury, Gregory Chanan, Trevor Killeen, Zeming Lin, Natalia Gimelshein, Luca Antiga, et al. Pytorch: An imperative style, high-performance deep learning library. *Advances in Neural Information Processing Systems*, 32, 2019.

Boris Polyak. Some methods of speeding up the convergence of iteration methods. *USSR Computational Mathematics and Mathematical Physics*, 4(5):1–17, 1964. ISSN 0041-5553.

Sashank J. Reddi, Satyen Kale, and Sanjiv Kumar. On the convergence of adam and beyond. In *International Conference on Learning Representations*, 2018.

Herbert Robbins and Sutton Monro. A stochastic approximation method. *The annals of mathematical statistics*, pp. 400–407, 1951.

David E. Rumelhart, Geoffrey Hinton, and Ronald J. Williams. Learning internal representations by error propagation, parallel distributed processing, explorations in the microstructure of cognition, ed. de rumelhart and j. mcclelland. vol. 1. 1986. *Biometrika*, 71(599-607):6, 1986.

Olga Russakovsky, Jia Deng, Hao Su, Jonathan Krause, Sanjeev Satheesh, Sean Ma, Zhiheng Huang, Andrej Karpathy, Aditya Khosla, Michael Bernstein, et al. Imagenet large scale visual recognition challenge. *International journal of computer vision*, 115:211–252, 2015.

John Schulman, Filip Wolski, Prafulla Dhariwal, Alec Radford, and Oleg Klimov. Proximal policy optimization algorithms. *arXiv preprint arXiv:1707.06347*, 2017.

Karen Simonyan and Andrew Zisserman. Very deep convolutional networks for large-scale image recognition. *arXiv preprint arXiv:1409.1556*, 2014.

Leslie N. Smith. A disciplined approach to neural network hyper-parameters: Part 1–learning rate, batch size, momentum, and weight decay. *arXiv preprint arXiv:1803.09820*, 2018.

Samuel Smith, Erich Elsen, and Soham De. On the generalization benefit of noise in stochastic gradient descent. In *International Conference on Machine Learning*, pp. 9058–9067. PMLR, 2020.

Ilya Sutskever, James Martens, George Dahl, and Geoffrey Hinton. On the importance of initialization and momentum in deep learning. In Sanjoy Dasgupta and David McAllester (eds.), *Proceedings of the 30th International Conference on Machine Learning*, volume 28 of *Proceedings of Machine Learning Research*, pp. 1139–1147, Atlanta, Georgia, USA, 17–19 Jun 2013. PMLR.

Tijmen Tieleman and Geoffrey Hinton. Rmsprop: divide the gradient by a running average of its recent magnitude. *COURSERA: Neural Networks for Machine Learning*, 13, 2012.

Emanuel Todorov, Tom Erez, and Yuval Tassa. Mujoco: A physics engine for model-based control. In *2012 IEEE/RSJ International Conference on Intelligent Robots and Systems*, pp. 5026–5033. IEEE, 2012.

Bryan Van Scoy, Randy A Freeman, and Kevin M Lynch. The fastest known globally convergent first-order method for minimizing strongly convex functions. *IEEE Control Systems Letters*, 2(1): 49–54, 2017.

Ashish Vaswani, Noam Shazeer, Niki Parmar, Jakob Uszkoreit, Llion Jones, Aidan N Gomez, Łukasz Kaiser, and Illia Polosukhin. Attention is all you need. *Advances in Neural Information Processing Systems*, 2017.

Runzhe Wang, Sadhika Malladi, Tianhao Wang, Kaifeng Lyu, and Zhiyuan Li. The marginal value of momentum for small learning rate SGD. In *The Twelfth International Conference on Learning Representations*, 2024.

Jiayi Weng, Huayu Chen, Dong Yan, Kaichao You, Alexis Duburcq, Minghao Zhang, Yi Su, Hang Su, and Jun Zhu. Tianshou: A highly modularized deep reinforcement learning library. *Journal of Machine Learning Research*, 23(267):1–6, 2022.

Sam Wiseman and Alexander M. Rush. Sequence-to-sequence learning as beam-search optimization. *Proceedings of the 2016 Conference on Empirical Methods in Natural Language Processing*, 2016.

Felix Wu, Angela Fan, Alexei Baevski, Yann N Dauphin, and Michael Auli. Pay less attention with lightweight and dynamic convolutions. *International Conference on Learning Representations*, 2019.

Yan Yan, Tianbao Yang, Zhe Li, Qihang Lin, and Yi Yang. A unified analysis of stochastic momentum methods for deep learning. *Proceedings of the Twenty-Seventh International Joint Conference on Artificial Intelligence*, 2018.

Hao Yu, Rong Jin, and Sen Yang. On the linear speedup analysis of communication efficient momentum sgd for distributed non-convex optimization. In *International Conference on Machine Learning*, pp. 7184–7193. PMLR, 2019.

Lotfi A. Zadeh. Frequency analysis of variable networks. *Proceedings of the IRE*, 38(3):291–299, 1950.

Lotfi A. Zadeh. Time-varying networks, i. *Proceedings of the IRE*, 49(10):1488–1503, 1961.

A ADDITIONAL DERIVATIONS AND PROOF

A.1 DERIVATION OF EQUATION (8)

$$\begin{aligned}
|H_k(\omega)| &= \sqrt{H_k(\omega)H_k^\dagger(\omega)} \\
&= \sqrt{\frac{v_k}{1-u_k e^{-j\omega}} \cdot \frac{v_k}{1-u_k e^{j\omega}}} \\
&= \sqrt{\frac{v_k^2}{1-u_k e^{-j\omega} - u_k e^{j\omega} + u_k^2 e^{-j\omega} e^{j\omega}}} \\
&= \sqrt{\frac{v_k^2}{1-u_k(\cos\omega - j\sin\omega) - u_k(\cos\omega + j\sin\omega) + u_k^2(\cos^2\omega + \sin^2\omega)}} \\
&= \sqrt{\frac{v_k^2}{1-2u_k\cos\omega + u_k^2}} \\
&= \frac{|v_k|}{\sqrt{1-2u_k\cos\omega + u_k^2}}
\end{aligned}$$

A.2 DERIVATION OF EQUATION (9)

$$\begin{aligned}
\arg(H_k(\omega)) &= \arg(v_k) - \arg(1-u_k e^{-j\omega}) \\
&= \arg(v_k) - \arg\left((1-u_k\cos\omega) + j(u_k\sin\omega)\right) \\
&= \arg(v_k) - \tan^{-1}\left(\frac{u_k\sin\omega}{1-u_k\cos\omega}\right)
\end{aligned}$$

A.3 PROOF OF PROPOSITION 1

According to Algorithm 1, the momentum coefficient in the k-th stage ($k = 1, 2, \cdots, N$) is

$$u_k = \frac{(k-1)\delta}{(k-1)\delta + \mu} = \frac{(k-1)\delta}{(k-1)\delta + \Sigma/c} = \frac{(k-1)\delta}{(k-1)\delta + cN\delta} = \frac{k-1}{k-1+cN}. \tag{12}$$

This guarantees that the number of training steps, which may be different when choosing other training strategies or changing datasets, is independent of u_k when the scaling factor c and the number of stages N are already determined.

B ADDITIONAL EXPERIMENTS

In this section, we present several supplementary experiments. The detailed experimental settings are shown in App. C.

B.1 DYNAMIC SEQUENCE CONSTRUCTION

There are infinite increasing or decreasing sequences. In this part, we compare the test set performance of the sequence mentioned in Equ. 4 with four other dynamic sequences. Specifically, we compare with the following four dynamic increasing sequences within Algorithm 1:

Linear: $u(t) = a_1 t$;
Exponential: $u(t) = 1 - e^{-a_2 t}$;
Sine: $u(t) = \sin(a_3 t)$;
Logarithmic: $u(t) = \ln(a_4 t)$;

where a_1 to a_4 are scaling coefficients. For a fair comparison, we adjust the coefficients to keep the u_t of all sequences unchanged in the beginning and ending stages. To make other types of sequences unique, we keep the u_t of different dynamic sequences nearly unchanged in the beginning and ending stages. Table 5 displays their test accuracy results after 300 epochs of training on CIFAR-100 using ResNet50. We ran each experiment under 3 different random seeds (0, 1, 2). Clearly, the dynamic sequence we use in Equ. 4 shows its superiority over other constructions.

Table 5: Top-1 ACC. (%) comparisons of using linear, exponential, sine, logarithmic, and our sequences when adopting FSGDM.

Dynamic Sequence Type	Ours	Linear	Exponential	Sine	Logarithmic
ACC-1 (%)	$\mathbf{81.44}_{0.06}$	$78.24_{0.24}$	$80.38_{0.04}$	$78.76_{0.29}$	$78.70_{0.09}$

Specifically, $(a_1, a_2, a_3, a_4) = (8.271 \times 10^{-6}, 3.793 \times 10^{-5}, 1.125 \times 10^{-5}, 1.394 \times 10^{-5})$.

B.2 ADDITIONAL FIGURES OF HIGH-PASS MOMENTUM SYSTEMS ON CIFAR-100

This subsection provides the figures of the dynamic magnitude responses and norm of high-pass (gain) momentum systems mentioned in Sec. 3. Fig. 6 and Fig. 7 show the magnitude responses and norm comparisons of high-pass and high-pass gain momentum systems, respectively. The high-pass (gain) momentum systems preserve or even amplify rapidly fluctuating gradient components, leading to sharp oscillations in gradient norm curves and momentum norm curves across iterations.

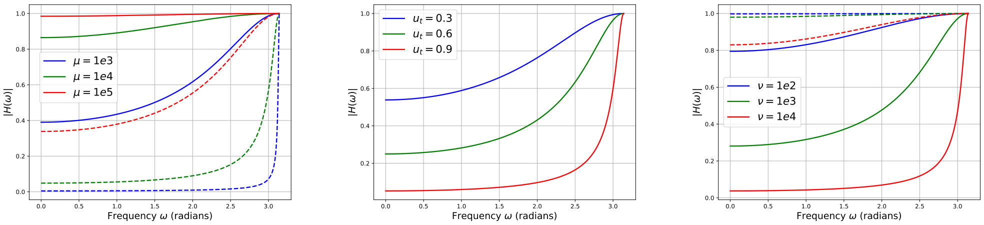

(a) Dynamic Magnitude Response (b) Magnitude Response (c) Dynamic Magnitude Response

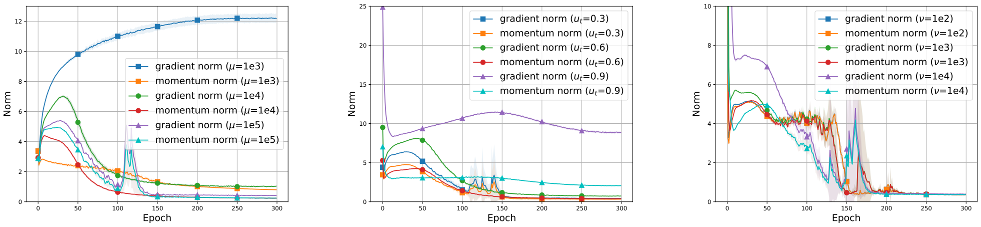

(d) Norm Comparisons (e) Norm Comparisons (f) Norm Comparisons

Figure 6: (**Up**) Analysis of the (dynamic) magnitude responses in the early and late training stages for EMA-SGDM with high-pass momentum defined in Eqn. 10. The *solid lines* denote the magnitude responses in the *early stages*, and the *dashed lines* denote the magnitude responses in the *late stages*. (**Down**) The comparison between the gradient norms and momentum norms for EMA-SGDM with high-pass momentum. Left Column: increasing sequence. Middle Column: fixed sequence. Right Column: decreasing sequence.

B.3 ADDITIONAL EXPERIMENTS OF VGG16 ON CIFAR-10

In this subsection, we provide experiments of training VGG16 on CIFAR-10. The experimental settings follow Sec. 3 and App. C. From the test accuracy in Table 6 and Table 7, we observe that the test performances and norm comparisons in different momentum methods in training VGG16 on

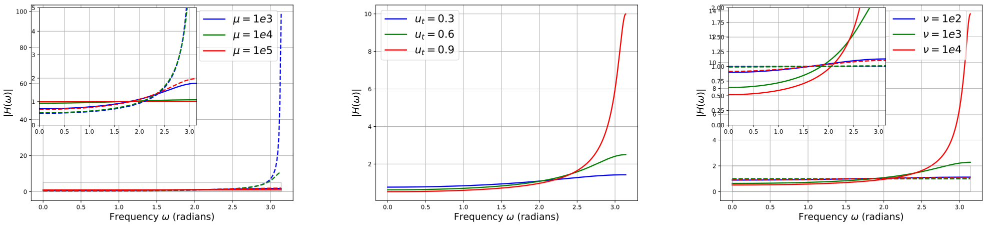

(a) Dynamic Magnitude Response (b) Magnitude Response (c) Dynamic Magnitude Response

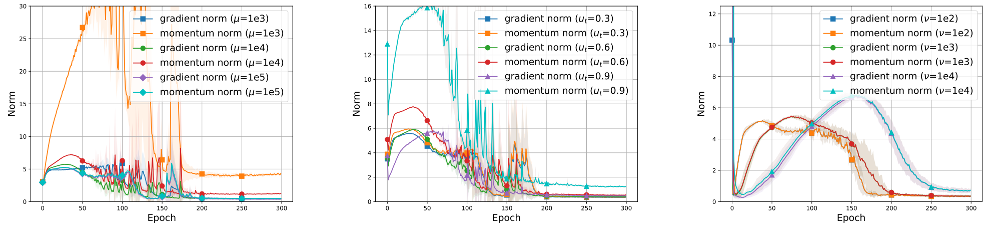

(d) Norm Comparisons (e) Norm Comparisons (f) Norm Comparisons

Figure 7: (**Up**) Analysis of the (dynamic) magnitude responses in the early and late training stages for Standard-SGDM with high-pass gain momentum defined in Eqn. 11. The *solid lines* denote the magnitude responses in the *early stages*, and the *dashed lines* denote the magnitude responses in the *late stages*. (**Down**) The comparison between the gradient norms and momentum norms for Standard-SGDM with high-pass gain momentum. Left Column: increasing sequence. Middle Column: fixed sequence. Right Column: decreasing sequence.

CIFAR-10 are similar to those in training ResNet50 on CIFAR-100. This similarity implies that the empirical findings in Sec. 3 are applicable to various CNNs.

Table 6: Comparison of Top-1 Accuracy (%) among different momentum coefficient methods in orthodox momentum systems using VGG16 on CIFAR-10.

	Increasing Factor (μ)			Fixed Value (u_t)			Decreasing Factor (ν)		
Parameters	1k	10k	100k	0.3	0.6	0.9	100	1k	10k
Low-Pass	$93.80_{0.05}$	$93.78_{0.12}$	$93.79_{0.09}$	$93.68_{0.18}$	$93.64_{0.08}$	$93.71_{0.07}$	$92.33_{0.04}$	$90.89_{0.11}$	$90.56_{0.19}$
High-Pass	$90.02_{0.05}$	$92.64_{0.09}$	$93.41_{0.01}$	$93.52_{0.16}$	$92.71_{0.07}$	$90.32_{0.07}$	$93.86_{0.09}$	$93.73_{0.08}$	$93.38_{0.09}$

Table 7: Comparison of Top-1 Accuracy (%) among different momentum coefficient methods in unorthodox momentum systems using VGG16 on CIFAR-10.

	Increasing Factor (μ)			Fixed Value (u_t)			Decreasing Factor (ν)		
Parameters	1k	10k	100k	0.3	0.6	0.9	100	1k	10k
Low-Pass Gain	$84.01_{0.13}$	$94.19_{0.07}$	$93.85_{0.07}$	$93.86_{0.11}$	$93.98_{0.09}$	$94.08_{0.07}$	$92.00_{0.05}$	$92.27_{0.12}$	$92.97_{0.23}$
High-Pass Gain	$93.34_{0.03}$	$93.56_{0.06}$	$93.79_{0.13}$	$93.71_{0.11}$	$93.46_{0.06}$	$93.33_{0.02}$	$93.79_{0.07}$	$93.33_{0.12}$	$93.05_{0.08}$

B.4 THE EARLY STAGES OF TRAINING

This subsection focuses on the test performance affected by the momentum coefficients in the very early training stages. We plot the test accuracy curves for the first 10 epochs of different momentum systems in Sec. 3 and study the early behaviors of different momentum systems.

Fig. 8 demonstrates the early test accuracy curves of different momentum coefficient methods. For orthodox momentum systems, preserving the original gradient (i.e., all-pass momentum system,

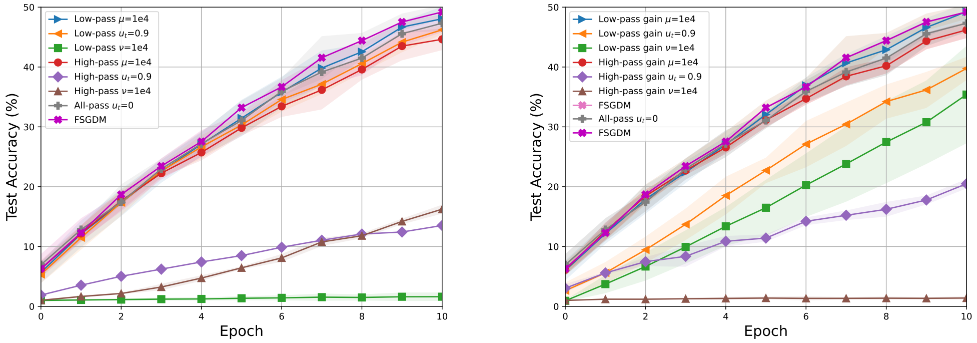

(a) Orthodox Momentum Systems (b) Unorthodox Momentum Systems

Figure 8: The first 10 epochs of the test accuracy curves with different momentum coefficient methods. We choose 10^4 for both increasing and decreasing factors (μ and ν) in dynamic momentum systems and $u_t = 0.9$ for static momentum coefficient.

low-pass momentum system with an increasing u_t, and high-pass momentum system with an increasing u_t) or attenuating high-frequency gradient components(i.e., static low-pass momentum system with $u_t = 0.9$) results in better initial performance, while greatly attenuating high-frequency gradient components (i.e., low-pass momentum system with a decreasing u_t) or attenuating low-pass components (i.e., static high-pass and high-pass momentum system with a decreasing u_t) lead to bad test performance at the beginning.

On the other hand, for unorthodox momentum systems, preserving the original gradient (i.e., all-pass momentum system, low-pass gain momentum system with an increasing u_t, and high-pass gain momentum system with an increasing u_t) can achieve better early performance, while greatly amplifying high-frequency gradient components (i.e., static high-pass gain momentum system and high-pass gain momentum system with a decreasing u_t) leads to bad initial accuracy results.

These observations significantly validate that preserving the original gradient in early stages enhances test performance, which matches the findings in Sec. 3. Additionally, our proposed FSGDM retains the all-pass characteristic and possesses the same quick start property in test accuracy curves.

B.5 COMPARISON WITH SPECIAL MOMENTUM SYSTEMS

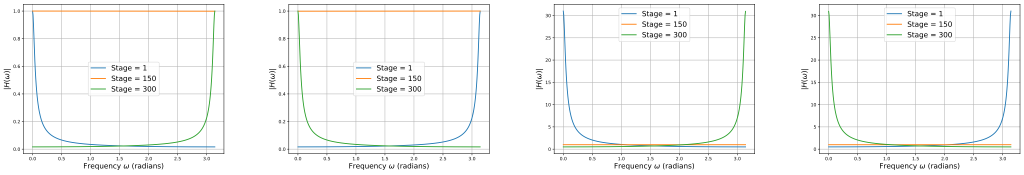

(a) LP2HP (b) HP2LP (c) LPG2HPG (d) HPG2LPG

Figure 9: The magnitude response curves of Stage $1, 150, 300$ in different momentum systems.

In this subsection, we investigate the test performance of the following four types of momentum systems: 1) low-pass to high-pass momentum system (LP2HP); 2) high-pass to low-pass momentum system (HP2LP); 3) low-pass gain to high-pass gain momentum system (LPG2HPG); 4) high-pass gain to low-pass gain momentum system (HPG2LPG). Their dynamic magnitude responses are shown in Fig. 9. Note that the maximum values $|H(\omega)|$ of these four systems are the same as the default setting in FSGDM. We run each experiment under 3 different random seeds (0-2). Table 8 displays the test accuracy results of four types of momentum systems and FSGDM. Clearly, our proposed FSGDM outperforms all four special momentum systems. Specifically, the test accuracy of the momentum systems shifting from high-pass to low-pass is better than that shifting from low-pass to high-pass. This indicates that compared to the low-frequency gradient components, high-frequency components are more undesired in the late training stages, which supports the finding in Sec. 3.

Table 8: Comparison of Top-1 Accuracy (%) among the low-pass to high-pass, high-pass to low-pass, low-pass gain to high-pass gain, high-pass gain to low-pass gain momentum systems and FSGDM.

Dynamic Magnitude Response	FSGDM	LP2HP	HP2LP	LPG2HPG	HPG2LPG
ACC-1 (%)	$\mathbf{81.44}_{0.06}$	$74.77_{0.21}$	$77.00_{0.13}$	$72.60_{0.58}$	$78.91_{0.25}$

B.6 TRAINING WITH EXTREME MOMENTUM COEFFICIENTS

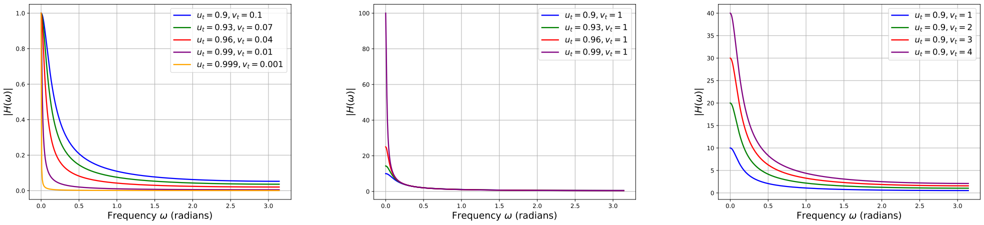

(a) Extreme u_t in EMA Setting (b) Extreme u_t with $v_t = 1$ (c) Extreme v_t with $u_t = 0.9$

Figure 10: The magnitude responses of different u_t and v_t with extreme value ranges. (a): EMA-SGDM; (b), (c): Standard-SGDM.

Why do researchers usually choose $u_t = 0.9$ or $v_t = 1$ instead of larger values? From the frequency domain perspective, we discover that 1) when u_t is extremely close to 1 in EMA-SGDM, the momentum system will behave like a super narrow low-pass filter, with an extreme reduction in most of the high-frequency gradient components; 2) when u_t is extremely close to 1 in Standard-SGDM, the momentum system will behave like a super narrow low-pass gain filter, with a reduction in high-frequency gradient components and high amplification in a narrow band of low-frequency gradient components; 3) when v_t is larger than 1 in Standard-SGDM, the attenuation of high-frequency gradient components is then reduced. We speculate that all these poor filtering characteristics of the momentum systems will lead to bad test performance. Fig. 10 displays the magnitude response of these three situations. As shown in Fig. 11, the test performance results validate our previous speculations and support our frequency domain analysis framework.

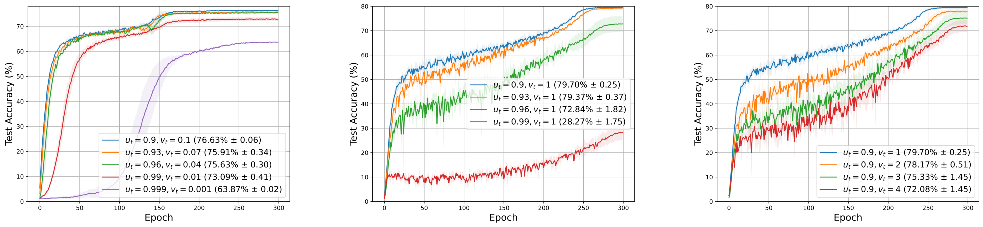

(a) Extreme u_t in EMA Setting (b) Extreme u_t with $v_t = 1$ (c) Extreme v_t with $u_t = 0.9$

Figure 11: The test accuracy curves of different u_t and v_t in extreme value ranges. (a): EMA-SGDM; (b), (c): Standard-SGDM.

B.7 ADDITIONAL EXPLORATION OF OPTIMAL SETTINGS FOR NLP TASKS

In this subsection, we provide experiments that explore the optimal parameter selection of FSGDM for the IWSLT14 translation task by training LSTM-W and Transformer-tiny. The experimental settings follow Sec. 5 and App. C.

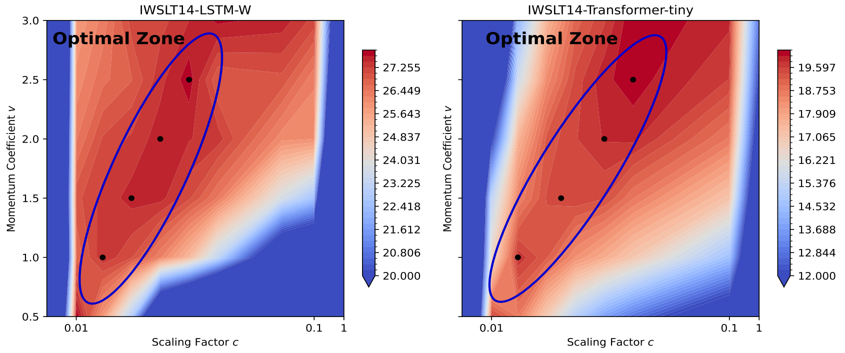

Figure 12: The BLEU scores of training LSTM-W and Transformer-tiny on IWSLT14 German-English translation task. The results show that the optimal parameter selections across these two training settings exhibit a high similarity. The black points denote the parameter selections with better test performance. The optimal zone of the parameter selection is circled in blue.

The results in Fig. 12 indicate that similar optimal zones can be observed on the NLP task. When the momentum coefficient v is fixed, the BLEU score shows an initial increase followed by a decline as the scaling factor c increases, which is highly consistent with the results in Sec. 4.2. In addition, we find that the empirical insights discussed in Sec. 3.3 are also applicable to various deep learning models beyond CNNs, as well as NLP tasks.

B.8 OPTIMAL ZONE OF FSGDM

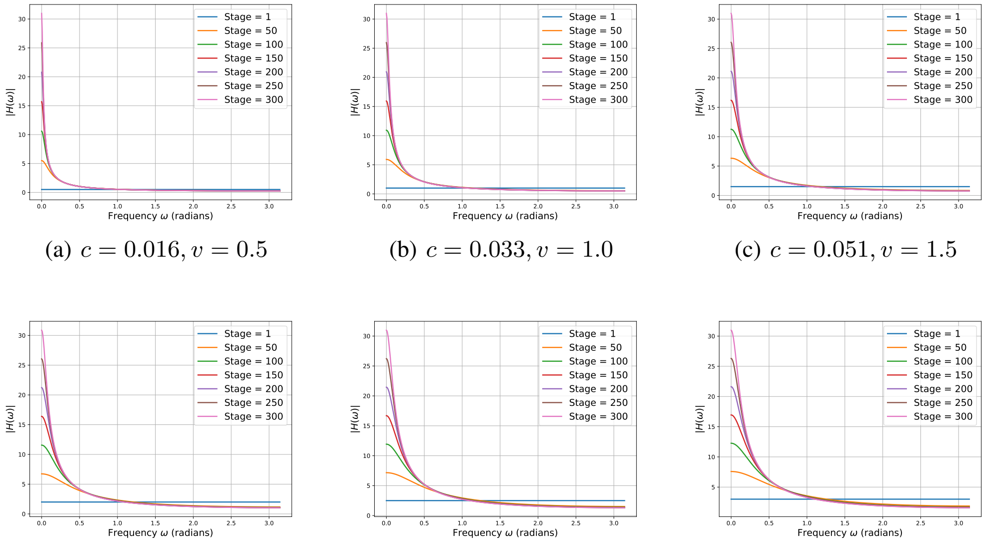

(a) $c = 0.016, v = 0.5$ (b) $c = 0.033, v = 1.0$ (c) $c = 0.051, v = 1.5$

(d) $c = 0.069, v = 2.0$ (e) $c = 0.088, v = 2.5$ (f) $c = 0.107, v = 3.0$

Figure 13: The dynamic magnitude responses of the black points in the optimal zone.

In this subsection, we delve further into the optimal zone. We suspect that the similarity of the dynamic magnitude responses may lead to close test set performance. The dynamic magnitude responses of the black points with different parameters in the optimal zone (Fig. 4) are shown in Fig. 13. We train ResNet50 on CIFAR-100 and visualize the training losses and the test accuracy curves of different points in the optimal zone. The results are shown in Fig. 14.

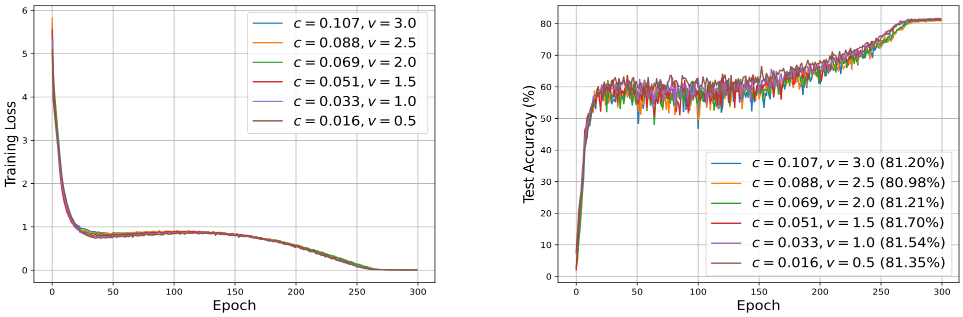

(a) Training Losses (b) Test Accuracy

Figure 14: The training losses and test accuracy of different parameter settings in the optimal zone.

From the training loss and test accuracy curves, we find that the optimization processes of different black points in the optimal zone resemble each other. According to the existing parameter settings of the black points, one can find that the mathematical relationship between c and v in training ResNet50 on CIFAR-100 is approximately $\frac{30.992}{v} \approx 1 + \frac{1}{c}$ [4].

B.9 ABLATION STUDY ON DIFFERENT BATCH SIZE

This subsection provides the experiments of training ResNet50 on CIFAR-100 with different batch size settings. We compare the Top-1 accuracy of the test set by using our FSGDM with $c = 0.033, v = 1$, Standard-SGDM with $u_t = 0.9, v_t = 1$, and EMA-SGDM with $u_t = 0.9$, as shown in Table 9. The test results show that our FSGDM consistently outperforms popular conventional SGD-based momentum optimizers.

Table 9: Comparison of Top-1 Accuracy (%) among the FSGDM, Standard-SGDM, and EMA-SGDM with different batch size settings.

Batch size	64	128	256
EMA-SGDM	$79.42_{0.11}$	$76.84_{0.06}$	$69.03_{0.39}$
Standard-SGDM	$79.55_{0.13}$	$79.71_{0.25}$	$78.96_{0.33}$
FSGDM	$\mathbf{80.92}_{0.13}$	$\mathbf{81.44}_{0.06}$	$\mathbf{80.34}_{0.01}$

C EXPERIMENTAL SETTINGS

C.1 TRAINING SETTINGS FOR VISION CLASSIFICATION TASKS

We use custom training code based on the PyTorch tutorial code for all our visual classification experiments (including the experiments in Sec. 3, Sec. 4.2 and Sec. 5) We choose the CosineAnnealingLR (Loshchilov & Hutter, 2016) as our training scheduler. Additionally, we set the learning rate as 1×10^{-1} for all experiments, while the weight decay is set as 5×10^{-4} for experiments on CIFAR-10, CIFAR-100 and Tiny-ImageNet, and 1×10^{-1} for ImageNet. All models we used are simply following their paper's original architecture, and adopt the weight initialization introduced by He et al. (2015). Additionally, we train 300 epochs for experiments on CIFAR-10 and CIFAR-100 and train 100 epochs for Tiny-ImageNet and ImageNet. We use a 128 batch size for experiments on

---

[4] This relationship can be better approximated and generalized with continued experimentations across diverse tasks.

CIFAR-10, CIFAR-100 and Tiny-ImageNet, and 256 for ImageNet. All experiments are conducted on RTX 4090 or A100 GPUs.

Data Augmentation. For experiments on CIFAR-10, CIFAR-100 and Tiny-ImageNet, we adopt PyTorch's RandomCrop, followed by random horizontal flips. Specifically, the random crop size is set to 32x32 for CIFAR-10 and CIFAR-100 and set to 64x64 for Tiny-ImageNet. For experiments on ImageNet, we adopt PyTorch's RandomResizedCrop, cropping to 224x224 followed by random horizontal flips. Test images use a fixed resize to 256x256 followed by a center crop to 224x224. At last, a data normalization is adopted to input images.

C.2 TRAINING SETTINGS FOR NATURAL LANGUAGE PROCESSING TASKS

All models used in our experiments are directly adopted from the FairSeq [5] framework. We retain the original architecture of each model and train all models for 100 epochs using a single NVIDIA RTX 4090 GPU. We set the maximum batch size to 4,096 tokens and apply gradient clipping with a threshold of 0.1. The baseline learning rate is set to 0.25, and for the optimizer, we use a weight decay of 0.0001.

C.3 TRAINING SETTINGS FOR REINFORCEMENT LEARNING TASKS

For the experiments in RL tasks, we do not make any changes except for replacing the original Adam optimizer with Standard-SGDM, EMA-SGDM and our proposed FSGDM. To ensure fairness, we use Tianshou's (Weng et al., 2022) default hyperparameters for PPO training. However, since SGD-based optimizers are highly sensitive to the learning rate, we conducted a search for suitable learning rates across the three games, ultimately setting 10^{-2}, 10^{-2} and 10^{-3} for Walker2d-v4, HalfCheetah-v4, and Ant-v4, respectively.

D CHALLENGES IN THE FREQUENCY DOMAIN ANALYSIS FOR ADAPTIVE OPTIMIZERS

Algorithm 2: RMSprop

```
Input $\beta_2$, $\epsilon$, $v_0$;
for each $t = 1, 2, \dots$ do
    $g_t = \nabla\mathcal{L}_t(x_{t-1}, \zeta_{t-1})$;
    $v_t = \beta_2 v_{t-1} + (1-\beta_2) g_t^2$;
    $x_t = x_{t-1} - \alpha_t g_t / (\sqrt{v_t} + \epsilon)$;
end
```

Algorithm 3: Adam

```
Input $\beta_1$, $\beta_2$, $\epsilon$, $m_0$,$v_0$;
for each $t = 1, 2, \dots$ do
    $g_t = \nabla\mathcal{L}_t(x_{t-1}, \zeta_{t-1})$;
    $m_t = \beta_1 m_{t-1} + (1-\beta_1) g_t$;
    $v_t = \beta_2 v_{t-1} + (1-\beta_2) g_t^2$;
    $\widehat{m_t} = \frac{m_t}{1-\beta_1^t}$, $\widehat{v_t} = \frac{v_t}{1-\beta_2^t}$;
    $x_t = x_{t-1} - \alpha_t \widehat{m_t} / (\sqrt{\widehat{v_t}} + \epsilon)$;
end
```

In this section, we make a discussion on the potential challenges for the extension of the frequency domain analysis framework to adaptive optimizers like RMSprop and Adam as shown in Algorithm 2 and 3. The first-moment estimate of Adam is in the form of EMA and thus acts as a low-pass filter. However, the second-moment estimate presents additional obstacles for frequency domain analysis in the following ways:

1. The second-moment estimates of Adam and RMSprop involve the squared gradient term g_t^2, resulting in nonlinearity that complicates the direct application of the Z-transform.
2. Adam introduces both the first- and second-moment estimates (m_t and v_t), and adopts $\widehat{m}_t/(\sqrt{\widehat{v}_t} + \epsilon)$ as the update step. This intricate interaction between m_t and v_t also makes the analysis more challenging.

At this stage, we suspect that our argument regarding the three insights discussed in Sec. 3.3 might be also applicable to other types of optimizers. However, how the different frequency gradient components in the model parameter updates are actually processed by the Adam optimizer remains unclear. We anticipate that resolving these issues will provide deeper insights.

---

[5] https://github.com/facebookresearch/fairseq